ELSEVIER

Physica C 353 (2001) 270–282

PHYSICA C

www.elsevier.nl/locate/physc

Effects of dilute nonmagnetic impurities on the $\mathbf{Q} = (\pi, \pi)$ spin-fluctuation spectrum in $YBa_2Cu_3O_7$

N. Bulut *

Department of Physics, Koç University, Istinye, 80860 Istanbul, Turkey

Received 13 October 2000; accepted 2 November 2000

Abstract

The effects of nonmagnetic impurities on the $\mathbf{Q} = (\pi, \pi)$ spin-fluctuation spectral weight $\mathrm{Im}\,\chi(\mathbf{Q}, \omega)$ are studied within the framework of the two-dimensional Hubbard model using the random phase approximation. In the first part of the paper, the effects of the nonmagnetic impurities on the magnetic susceptibility of the noninteracting ($U = 0$) system, $\chi_0(\mathbf{q}, \omega)$, are calculated with the self-energy and the vertex corrections using various forms of the effective electron-impurity interaction. Here, the range and the strength of the impurity potential are varied as well as the concentration of the impurities. It is shown that the main effect of dilute impurities on $\chi_0(\mathbf{Q}, \omega)$ is to cause a weak smearing. In the second part, $\mathrm{Im}\,\chi(\mathbf{Q}, \omega)$ is calculated for the interacting system. Here, the calculations are concentrated on the processes which involve the impurity scattering of the spin fluctuations with finite momentum transfers. Results are given for various values of the model parameters, and comparisons are made with the neutron scattering data on Zn substituted $YBa_2Cu_3O_7$.

PACS: 74.62.Dh; 74.72.Bk; 75.10.Lp; 74.25.-q

1. Introduction and the model

Zn substitution has been used as a probe of the electronic properties in the layered cuprates and has yielded important results. Small amount of Zn impurities lead to a strong suppression of d-wave pairing [1]. Resistivity measurements find that Zn impurities act as strong scatterers [2]. Local magnetic measurements on Zn substituted cuprates have also yielded valuable information [3,4]. It has been found that within the presence of Zn impurities the uniform susceptibility of $YBa_2Cu_3O_{7-\delta}$ follows a Curie-like temperature dependence.

Inelastic neutron scattering experiments find that Zn impurities cause important changes in the $\mathbf{Q} \equiv (\pi, \pi)$ spin-fluctuation spectrum [5–7]. The experiments have been carried out for 2% [5] and 0.5% [6] Zn concentrations. It is found that even 0.5% Zn substitution in $YBa_2Cu_3O_7$ induces a peak in $\mathrm{Im}\,\chi(\mathbf{Q}, \omega)$ at $\omega = 40$ meV in the normal state [6]. The ω width of the peak is about 10 meV and its width in momentum space is resolution limited. This peak becomes observable below 250 K and its intensity continues to increase as T is lowered through $T_c = 87$ K. These results are quite different than those on pure $YBa_2Cu_3O_7$, where the peak is observed only in the superconducting state [8–10]. While in the case of 0.5% Zn substitution, no spectral weight is observed below

* Tel.: +90-212-338-1570; fax: +90-212-338-1559.
E-mail address: nbulut@ku.edu.tr (N. Bulut).

0921-4534/01/$ - see front matter
PII: S0921-4534(00)01758-5

$\sim$35 meV, in the 2% Zn substituted sample there is significant amount of spectral weight down to 5 meV. In this case, there is also a broad peak at 35 meV. The momentum width of this peak is 0.5 $\mathring{A}^{-1}$, which is about twice that of the peak in the 0.5% Zn substituted and the pure samples. Hence, the two main features induced in $\mathrm{Im}\,\chi(\mathbf{Q},\omega)$ in the normal state are the peak and the low frequency spectral weight observed in the 2% Zn substituted sample. Both of these features become observable already above T_c. The calculations reported in this article were motivated by these two effects on the frequency dependence of $\mathrm{Im}\,\chi(\mathbf{Q},\omega)$ in $YBa_2Cu_3O_7$ in the normal state.

Here, the results of diagrammatic calculations on the effects of nonmagnetic impurities on $\mathrm{Im}\,\chi(\mathbf{Q},\omega)$ obtained using the framework of the two-dimensional Hubbard model will be given. In the first part of the paper, the effects of various types of effective electron-impurity interactions on the magnetic susceptibility of the noninteracting ($U=0$) system, $\chi_0(\mathbf{Q},\omega)$, will be calculated. In this case, both the strength and the range of the impurity interaction, in addition to the concentration of impurities, will be varied. It will be found that in all these cases the main effect of impurity scattering is to cause a weak smearing of the structure in $\chi_0(\mathbf{Q},\omega)$. Hence, at this level, if χ_0 is used in an RPA expression, $\chi(\mathbf{Q},\omega)=\chi_0(\mathbf{Q},\omega)/(1-U\chi_0(\mathbf{Q},\omega))$, then one obtains a smearing of $\mathrm{Im}\,\chi(\mathbf{Q},\omega)$ by the impurity scattering rather than an enhancement as seen in the experiments. Here, it will be also noted that, for 2% impurity concentration, scattering from an extended impurity potential could induce spectral weight at low frequencies.

In the next part of the paper, the effects of the processes where the spin fluctuations are scattered by the impurities with finite momentum transfers are calculated. This type of processes will be called the "umklapp" processes, since they involve the scattering of the spin fluctuations by the impurity potential with finite momentum transfers as in the case of the scattering of the spin fluctuations by a charge-density-wave field. In this part, the effects of the umklapp scatterings will be estimated by calculating the irreducible off-diagonal susceptibility $\chi_0(\mathbf{q},\mathbf{q}',\omega)$, where $\mathbf{q}\neq\mathbf{q}'$, in the lowest order in the strength of the impurity potential. It will be seen that the important umklapp processes are the ones which involve the transfer of momentum $2\mathbf{k}_F$ to the spin fluctuations, and that they could lead to a peak in $\mathrm{Im}\,\chi(\mathbf{Q},\omega)$ at the frequency ω_0 which corresponds to the upper cut-off of the particle-hole continuum for $\mathbf{q}=(\pi,\pi)-2\mathbf{k}_F$. Here, $\mathbf{k}_F$ is the Fermi wave vector, and for the simple tight-binding band structure ω_0 corresponds to $2|\mu|$ where μ is the chemical potential. The underlying reason for this is a kinematic constraint which prohibits the creation of a particle-hole pair with center of mass momentum $\mathbf{q}=(\pi,\pi)-2\mathbf{k}_F$ and energy $\omega>\omega_0$. This constraint causes a nearly singular structure in $\chi_0(\mathbf{Q},\mathbf{q},\omega)$ at $\omega=\omega_0$, which in turn could lead to a peak in $\mathrm{Im}\,\chi(\mathbf{Q},\omega)$ at ω_0. Here, results will be given for various sets of the model parameters. It will be shown that these processes can lead to finite spectral weight at low frequencies as well. These results suggest that the umklapp scatterings could play a role in determining the effects of the impurities on the $\mathbf{Q}=(\pi,\pi)$ spin dynamics.

The starting point is the two-dimensional single-band Hubbard model given by

$$H=-t\sum_{\langle ij\rangle,\sigma}(c^{\dagger}_{i\sigma}c_{j\sigma}+c^{\dagger}_{j\sigma}c_{i\sigma})+U\sum_i c^{\dagger}_{i\uparrow}c_{i\uparrow}c^{\dagger}_{i\downarrow}c_{i\downarrow}-\mu\sum_{i,\sigma}c^{\dagger}_{i\sigma}c_{i\sigma}, \tag{1}$$

which will be used to model the spin fluctuations of the pure system. Here $c_{i\sigma}$ ($c^{\dagger}_{i\sigma}$) annihilates (creates) an electron with spin σ at site i, t is the near-neighbor hopping matrix element and U is the onsite Coulomb repulsion. For simplicity, the hopping t, the lattice constant a and $\hbar$ are set to 1.

Within the presence of an impurity, the magnetic susceptibility is defined by

$$\chi(\mathbf{q},\mathbf{q}',i\omega_m)=\int_0^{\beta}\mathrm{d}\tau\,\mathrm{e}^{i\omega_m\tau}\langle m^-(\mathbf{q},\tau)m^+(\mathbf{q}',0)\rangle, \tag{2}$$

where $m^+(\mathbf{q})=N^{-1/2}\sum_{\mathbf{p}}c^{\dagger}_{\mathbf{p}+\mathbf{q}\uparrow}c_{\mathbf{p}\downarrow}$, $m^-(\mathbf{q})=(m^+(\mathbf{q}))^{\dagger}$, and $\omega_m=2m\pi T$. By letting $i\omega_m\rightarrow\omega+i\delta$, one obtains $\chi(\mathbf{q},\mathbf{q}',\omega)$. If one assumes that the effective interaction between an impurity and the electrons can be approximated by a static potential, then the RPA expression for the magnetic susceptibility becomes

$$\chi(\mathbf{q},\mathbf{q}',\omega)=\chi_0(\mathbf{q},\mathbf{q}',\omega)+U\sum_{\mathbf{q}''}\chi_0(\mathbf{q},\mathbf{q}'',\omega)\chi(\mathbf{q}'',\mathbf{q}',\omega), \quad (3)$$

where $\chi_0(\mathbf{q},\mathbf{q}',\omega)$ is the irreducible susceptibility dressed with the impurity scatterings. The off-diagonal $\mathbf{q}\neq\mathbf{q}'$ terms of $\chi_0(\mathbf{q},\mathbf{q}',\omega)$ vanish for the pure system, but they are finite within the presence of impurity scattering. After obtaining $\chi(\mathbf{q},\mathbf{q}',\omega)$ from Eq. (3) for one impurity, the averaging over the impurity location can be done, which sets $\mathbf{q}=\mathbf{q}'$. Finally, $\chi(\mathbf{q},\mathbf{q},\omega)$ obtained this way can be scaled to the case of a finite concentration of impurities. Note that this approach neglects the interactions between the impurities, and it would be valid only in the dilute limit. In the following, for simplicity, $\chi(\mathbf{q},\mathbf{q},\omega)$ and $\chi_0(\mathbf{q},\mathbf{q},\omega)$ will be denoted by $\chi(\mathbf{q},\omega)$ and $\chi_0(\mathbf{q},\omega)$, respectively.

In solving Eq. (3), if the off-diagonal terms are omitted, then one obtains

$$\chi(\mathbf{q},\omega)=\frac{\chi_0(\mathbf{q},\omega)}{1-U\chi_0(\mathbf{q},\omega)}, \quad (4)$$

where $\chi_0(\mathbf{q},\omega)$ is dressed with the impurity scatterings. In the next section, $\chi_0(\mathbf{Q}=(\pi,\pi),\omega)$ will be calculated using various impurity potentials. In the third section, $\chi(\mathbf{Q},\omega)$ will be calculated without omitting the off-diagonal terms in Eq. (3).

2. Effects of the nonmagnetic impurities without the umklapp scatterings

In this part, the effects of dilute nonmagnetic impurities on the magnetic susceptibility of the noninteracting ($U=0$) system will be calculated using various impurity potentials. The method used here for calculating $\chi_0(\mathbf{Q},\omega)$ is similar to those used in Refs. [11–13]. Both the self-energy and the vertex corrections induced by the impurity scattering will be included [14,15].

In Refs. [16–18], it has been shown how the electronic correlations lead to an extended effective interaction between an impurity and the electrons. The extended nature of the effective impurity potential has been also emphasized in Ref. [19]. Assuming that it can be approximated by a static form, the potential due to an impurity at site $\mathbf{r}_0$ can be written as

$$V_{\text{eff}}=\sum_{v\alpha\sigma}V_{v\alpha}c^{\dagger}_{v\alpha\sigma}c_{v\alpha\sigma}, \quad (5)$$

where v denotes the distance from the impurity and α denotes the different partial wave components. The single-particle operators $c_{v\alpha\sigma}$ are given by

$$c_{v\alpha\sigma}=\sum_{\mathbf{d}_v}g_{v\alpha}(\mathbf{d}_v)c_{\sigma}(\mathbf{r}_0+\mathbf{d}_v), \quad (6)$$

where $\mathbf{d}_v$ sums over the sites at a distance v away from the impurity and $g_{v\alpha}(\mathbf{d}_v)$'s are the coefficients of the partial-wave components. In the following, an impurity interaction with a range of $\sqrt{2}$ lattice spacings, which includes the second near-neighbor site, will be considered. For simplicity, subscript i will be used to denote both v and α.

Within the presence of impurity scattering, the single-particle Green's function defined by

$$G(\mathbf{p},\tau)=-\langle T_{\tau}c_{\mathbf{p}\sigma}(\tau)c^{\dagger}_{\mathbf{p}\sigma}(0)\rangle \quad (7)$$

is obtained from

$$G(\mathbf{p},i\omega_n)=G_0(\mathbf{p},i\omega_n)+n_i(G_0(\mathbf{p},i\omega_n))^2\times\sum_{ij}g_i(\mathbf{p})T_{ij}(i\omega_n)g_j(\mathbf{p}), \quad (8)$$

where n_i is the concentration of the impurities and the Matsubara frequency $\omega_n=(2n+1)\pi T$. For an impurity potential with a range of $\sqrt{2}$ lattice spacings, the subscripts i and j vary from 1 to 9. The single-particle Green's function of the pure system $G_0(\mathbf{p},i\omega_n)$ entering Eq. (8) is given by

$$G_0(\mathbf{p},i\omega_n)=\frac{1}{i\omega_n-\varepsilon_{\mathbf{p}}}, \quad (9)$$

where the single-particle dispersion relation is

$$\varepsilon_{\mathbf{p}}=-2t(\cos p_x+\cos p_y)-\mu. \quad (10)$$

The terms contributing to $G(\mathbf{p},i\omega_n)$ are illustrated diagrammatically in Fig. 1(a). In Eq. (8), $T_{ij}(i\omega_n)$ is the impurity-scattering t-matrix and $g_i(\mathbf{p})$'s are the form factors which are given by

$$g_i(\mathbf{p})=\sum_{\mathbf{d}_v}g_{v\alpha}(\mathbf{d}_v)e^{i\mathbf{p}\mathbf{d}_v}, \quad (11)$$

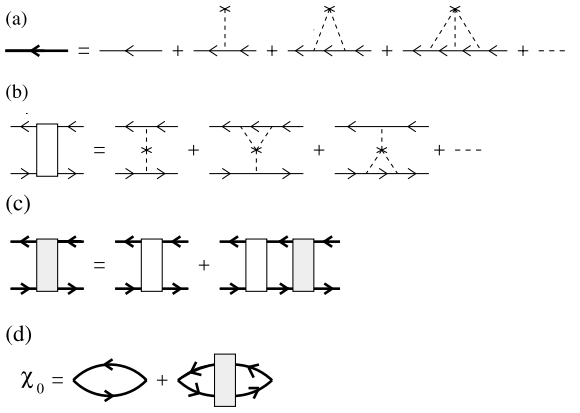

Fig. 1. (a) Feynman diagrams for the single-particle Green's function dressed with the impurity scatterings. (b) Irreducible vertex Γ^0 in the particle-hole channel arising from the impurity scattering. (c) Reducible vertex Γ in the particle-hole channel given in terms of Γ^0. (d) Irreducible magnetic susceptibility $\chi_0(\mathbf{Q}, i\omega_m)$ dressed with the impurity-induced self-energy and vertex corrections.

where i denotes (ν, α). The first five of the nine form factors used here are

$$\begin{aligned} g_{0s}(\mathbf{p}) &= 1, \\ g_{1s}(\mathbf{p}) &= \cos p_x + \cos p_y, \\ g_{1p_x}(\mathbf{p}) &= 2\sin p_x, \\ g_{1p_y}(\mathbf{p}) &= 2\sin p_y, \\ g_{1d}(\mathbf{p}) &= \cos p_x - \cos p_y, \end{aligned} \tag{12}$$

with similar expressions for the remaining $\alpha = \sqrt{2}$ components having s, p_x, p_y and d-wave symmetries. The t-matrix $T_{ij}(i\omega_n)$ is obtained by solving

$$T_{ij}(i\omega_n) = \delta_{ij} V_i + V_i \sum_{\ell} F_{i\ell}(i\omega_n) T_{\ell j}(i\omega_n), \tag{13}$$

where

$$F_{ij}(i\omega_n) = \frac{1}{N} \sum_{\mathbf{p}} g_i(\mathbf{p}) G_0(\mathbf{p}, i\omega_n) g_j(\mathbf{p}). \tag{14}$$

In order to calculate $\chi_0(\mathbf{Q}, i\omega_m)$, the irreducible interaction Γ^0 in the particle-hole channel due to impurity scattering is needed. In Fig. 1(b), Γ^0 is illustrated diagrammatically and the corresponding expression is

$$\begin{aligned} &\Gamma^0_{ii',jj'}(\mathbf{p}, \mathbf{p}', i\omega_n, i\omega_m) \\ &\quad = -n_i g_i(\mathbf{p}) g_{i'}(\mathbf{p}+\mathbf{Q}) T_{ij}(i\omega_n) T_{i'j'}(i\omega_n + i\omega_m) g_j(\mathbf{p}') \\ &\qquad \times g_{j'}(\mathbf{p}'+\mathbf{Q}). \end{aligned} \tag{15}$$

Here, Γ^0 is evaluated with the center-of-mass momentum $\mathbf{Q} \equiv (\pi, \pi)$. Next, the reducible vertex in the particle-hole channel is obtained by solving

$$\begin{aligned} &\Gamma_{ii',jj'}(\mathbf{p}, \mathbf{p}', i\omega_n, i\omega_m) \\ &\quad = \Gamma^0_{ii',jj'}(\mathbf{p}, \mathbf{p}', i\omega_n, i\omega_m) \\ &\qquad - \sum_{\ell\ell',ss'} \frac{1}{N} \sum_{\mathbf{k}} \Gamma^0_{ii',\ell\ell'}(\mathbf{p}, \mathbf{k}, i\omega_n, i\omega_m) G(\mathbf{k}, i\omega_n) \\ &\qquad \times G(\mathbf{k}+\mathbf{Q}, i\omega_n + i\omega_m) \Gamma_{ss',jj'}(\mathbf{k}, \mathbf{p}', i\omega_n, i\omega_m), \end{aligned} \tag{16}$$

which is illustrated in Fig. 1(c). Here, it is noted that Γ^0 is calculated using the bare single-particle Green's function G_0, while Γ is calculated using the Green's function dressed with the impurity scatterings. This is necessary in order to prevent double-counting [15]. In terms of the reducible vertex, $\chi_0(\mathbf{Q}, i\omega_m)$ is given by

$$\begin{aligned} \chi_0(\mathbf{Q}, i\omega_m) = \overline{\chi}_0(\mathbf{Q}, i\omega_m) &- T \sum_{i\omega_n} \frac{1}{N} \sum_{\mathbf{p}} \frac{1}{N} \\ &\times {\sum_{\mathbf{p}'}}' G(\mathbf{p}+\mathbf{Q}, i\omega_n + i\omega_m) G(\mathbf{p}, i\omega_n) \\ &\times \sum_{ii',jj'} \Gamma_{ii',jj'}(\mathbf{p}, \mathbf{p}', i\omega_n, i\omega_m) \\ &\times G(\mathbf{p}'+\mathbf{Q}, i\omega_n + i\omega_m) G(\mathbf{p}', i\omega_n). \end{aligned} \tag{17}$$

Here, $\overline{\chi}_0(\mathbf{Q}, i\omega_m)$ includes only the impurity induced self-energy corrections, and it is given by

$$\begin{aligned} &\overline{\chi}_0(\mathbf{Q}, i\omega_m) \\ &\quad = -\frac{T}{N} \sum_{\mathbf{p}, i\omega_n} G(\mathbf{p}+\mathbf{Q}, i\omega_n + i\omega_m) G(\mathbf{p}, i\omega_n). \end{aligned} \tag{18}$$

These results in terms of the Matsubara frequencies are analytically continued to the real frequency axis by the Pade approximation. In the following, the results on $\chi_0(\mathbf{Q}, \omega)$ obtained this way will be compared with the Lindhard susceptibility of the pure system,

$$\chi_0^{\mathrm{L}}(\mathbf{Q},\omega)=\frac{1}{N}\sum_{\mathbf{p}}\frac{f(\varepsilon_{\mathbf{p}+\mathbf{Q}})-f(\varepsilon_{\mathbf{p}})}{\omega-(\varepsilon_{\mathbf{p}+\mathbf{Q}}-\varepsilon_{\mathbf{p}})+i\delta}. \tag{19}$$

Fig. 2 shows results obtained using a strongly attractive onsite impurity potential $V_0=-20$ and an impurity concentration of $n_i=0.02$. In addition, here filling $\langle n\rangle=0.875$ and temperature $T=0.02$ are used. In Fig. 2(a), $\chi_0(\mathbf{Q},i\omega_m)$ versus ω_m is shown. Also shown in this figure are $\overline{\chi}_0(\mathbf{Q},i\omega_m)$, which does not include the impurity vertex corrections, and the Lindhard susceptibility $\chi_0^{\mathrm{L}}(\mathbf{Q},i\omega_m)$ of the pure system. Fig. 2(b) and (c) show the corresponding real and imaginary parts obtained by the Pade analytic continuation. Here, one observes that the impurity-induced self-energy corrections suppress $\chi_0(\mathbf{Q},i\omega_m)$ and smear the structure in $\chi_0(\mathbf{Q},\omega)$. For instance, the hump in $\mathrm{Re}\,\chi_0^{\mathrm{L}}(\mathbf{Q},\omega)$ at $\omega\approx 2|\mu|=0.48$ is smeared by the self-energy corrections, but when the vertex corrections are included, the effect of the self-energy corrections is nearly canceled. This hump is because of a logarithmic singularity in $\mathrm{Re}\,\chi_0(\mathbf{Q},\omega)$ at $T=0$ originating from the dynamic nesting of the Fermi surface. In a real system, the deviations from the simple tight-binding model which has only near-neighbor hoppings would lead to a suppression of this hump. In addition, the scattering of the single-particle excitations by the spin-fluctuations would suppress it also. These calculations were repeated using $n_i=0.005$ instead of $n_i=0.02$, in which case the difference between χ_0 and χ_0^{L} becomes even smaller (not shown here).

Fig. 3 shows results also for $n_i=0.02$ and an onsite impurity potential but now with $V_0=-1$. One observes that in this case the impurities have a stronger effect on χ_0. In addition, it is noted that $\mathrm{Re}\,\chi_0(\mathbf{Q},\omega)$ for $\omega\sim 0.5$ is suppressed, and $\mathrm{Re}\,\chi_0(\mathbf{Q},\omega\sim 0)$ gets enhanced by a small amount. Among the various forms tried for the impurity potential, this is the only case where an enhancement of $\chi_0(\mathbf{Q},\omega)$ by the impurity scatterings has been obtained. This effect is due to the enhancement of the single-particle density of states at the impurity site by the attractive potential. The enhancement of $\mathrm{Re}\,\chi_0(\mathbf{Q},\omega\sim 0)$ at small frequencies could lead to some enhancement of the low-frequency antiferromagnetic spin fluctuations for a system with a large Stoner factor. However, it is seen that $\mathrm{Re}\,\chi_0(\mathbf{Q},\omega)$ for ω near $\omega_0=2|\mu|$ is suppressed. This calculation was repeated using $V_0=$

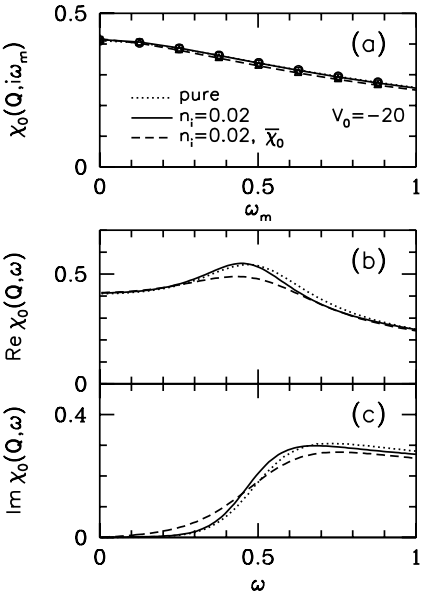

Fig. 2. Results on (a) $\chi_0(\mathbf{Q},i\omega_m)$ versus ω_m, (b) $\mathrm{Re}\,\chi_0(\mathbf{Q},\omega)$ versus ω and (c) $\mathrm{Im}\,\chi_0(\mathbf{Q},\omega)$ versus ω for an onsite impurity potential with $V_0=-20$ and impurity concentration $n_i=0.02$. These results were obtained for $\langle n\rangle=0.875$ and $T=0.02$.

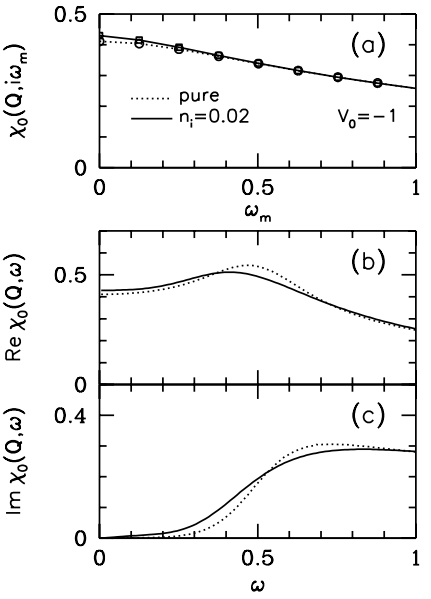

Fig. 3. Results similar to those in Fig. 2 but for $V_0=-1$.

1, and a suppresion of $\mathrm{Re}\,\chi_0(\mathbf{Q},\omega)$ was obtained due to the depletion of the single-particle density of states (not shown here).

Fig. 4 shows results on χ_0 obtained using an extended impurity potential for $n_i = 0.02$ and 0.005. These results were obtained for a potential with a range of $\sqrt{2}$ lattice spacings and with the following parameters: $V_{0s} = -20$, $V_{1\alpha} = 0.5$ and $V_{\sqrt{2}\alpha} = -0.25$ where α denotes the s, p_x, p_y and d-wave components. These values for $V_{\nu\alpha}$'s are comparable to those obtained in Ref. [19]. The calculations were repeated using various other values for the $V_{\nu\alpha}$'s, and it has been found that small changes in $V_{\nu\alpha}$'s do not change the results shown here significantly. For instance, increasing $V_{\nu\alpha}$'s by 50% does not change the conclusions of this section. In Fig. 4, it is seen that for $n_i = 0.02$ an extended potential leads to significant smearing of the structure in $\chi_0(\mathbf{Q},\omega)$. In this case, the hump in $\mathrm{Re}\,\chi_0(\mathbf{Q},\omega)$ is rounded off, and spectral weight is induced at low ω. Hence, comparing with Fig. 2, one observes that while an onsite impurity potential does not lead to spectral weight for $\omega < \omega_0$, an extended potential induces spectral weight at low ω. Also shown in Fig. 4 are the results for $n_i = 0.005$, in which case the effect of the impurities on $\chi_0(\mathbf{Q},\omega)$ is weaker. The fact that 0.5% impurities induce less spectral weight at low ω compared to the 2% case is consistent with the neutron scattering data by Refs. [5,6]. However, even for $n_i = 0.02$, the amount of the spectral weight induced at low ω is small. In the next section, it will be seen that the umklapp processes could also contribute to $\mathrm{Im}\,\chi(\mathbf{Q},\omega)$ at low ω.

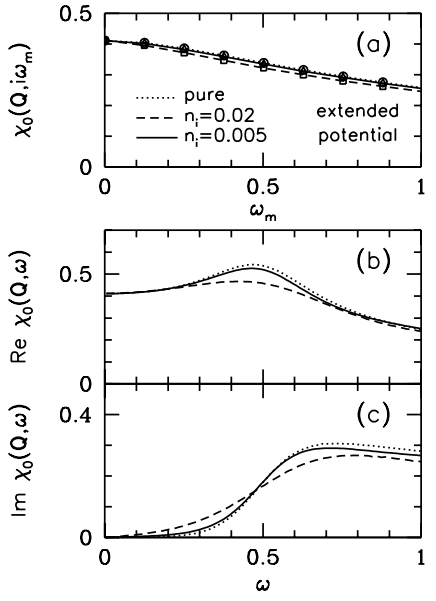

Fig. 4. Results similar to those in Fig. 2 but for an extended potential with the following set of parameters: $V_{0s} = -20$, $V_{1\alpha} = 0.5$ and $V_{\sqrt{2}\alpha} = -0.5$. Here results are given for both $n_i = 0.02$ and 0.005.

From the results presented here, one observes that if $\chi_0(\mathbf{Q},\omega)$ computed in this section is used in Eq. (4), then one would obtain mainly a smearing of $\mathrm{Im}\,\chi(\mathbf{Q},\omega)$ by the impurities. Hence, in this case, it would not be possible to explain how 0.5% Zn impurities induce a peak in $\mathrm{Im}\,\chi(\mathbf{Q},\omega)$ in the normal state of $YBa_2Cu_3O_7$.

3. Effects of the impurity induced umklapp scatterings

Here, $\mathrm{Im}\,\chi(\mathbf{Q},\omega)$ will be calculated without omitting the off-diagonal components in Eq. (3). These off-diagonal terms will be calculated in the lowest order in the strength of the impurity potential, as illustrated diagrammatically in Fig. 5(a). In the previous section, it was found that 0.5% and 2% impurities cause only a weak smearing of $\chi_0(\mathbf{Q},\omega)$. For this reason, the diagonal components of Eq. (3) will be approximated by the Lindhard susceptibility χ_0^{L}. This will not change the nearly singular contribution which could originate from the umklapp scatterings at $\omega \approx \omega_0$. The expression for $\chi_0(\mathbf{Q},\mathbf{q},i\omega_m)$ corresponding to the diagrams shown in Fig. 5(a) is

$$\chi_0(\mathbf{Q},\mathbf{q},i\omega_m) = -V_0\frac{T}{N}\sum_{\mathbf{p},i\omega_n}\{G_0(\mathbf{p}+\mathbf{Q},i\omega_n+i\omega_m) \times G_0(\mathbf{p},i\omega_n)G_0(\mathbf{p}+\mathbf{Q}-\mathbf{q},i\omega_n) + G_0(\mathbf{p},i\omega_n)G_0(\mathbf{p}+\mathbf{q},i\omega_n + i\omega_m)G_0(\mathbf{p}+\mathbf{Q},i\omega_n+i\omega_m)\}. \quad (20)$$

Here $\mathbf{Q} \equiv (\pi,\pi)$ and $\mathbf{q} = \mathbf{Q} - \mathbf{Q}^*$, where $\mathbf{Q}^*$ is the momentum transferred during the scattering from the impurity. Upon carrying out the summation

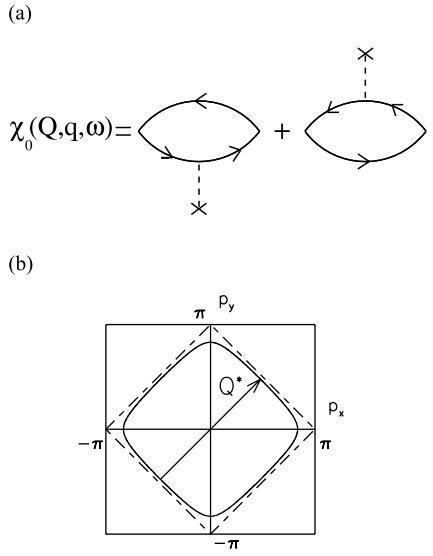

Fig. 5. (a) Feynman diagrams for the lowest-order terms contributing to the off-diagonal irreducible susceptibility $\chi_0(\mathbf{Q}, \mathbf{q}, \omega)$. (b) Sketch in the Brillouin zone of a quasiparticle scattering process where momentum $2\mathbf{k}_F$ is transferred.

over $i\omega_n$ in Eq. (20) and letting $i\omega_m \to \omega + i\delta$, one obtains

$$\chi_0(\mathbf{Q},\mathbf{q},\omega) = A(\mathbf{Q},\mathbf{q},\omega) + A^*(\mathbf{Q},\mathbf{q},-\omega) + B(\mathbf{Q},\mathbf{q},\omega) - B^*(\mathbf{Q},\mathbf{q},-\omega), \quad (21)$$

where '*' stands for complex conjugation, and A and B are given by

$$A(\mathbf{Q},\mathbf{q},\omega) = -\frac{V_{\mathbf{k}}}{N}\sum_{\mathbf{p}} \frac{1}{\varepsilon_{\mathbf{p}+\mathbf{Q}^*} - \varepsilon_{\mathbf{p}}} \times \left\{ \frac{f(\varepsilon_{\mathbf{p}+\mathbf{Q}^*})}{\omega - (\varepsilon_{\mathbf{p}+\mathbf{Q}} - \varepsilon_{\mathbf{p}+\mathbf{Q}^*}) + i\delta} - \frac{f(\varepsilon_{\mathbf{p}})}{\omega - (\varepsilon_{\mathbf{p}+\mathbf{Q}} - \varepsilon_{\mathbf{p}}) + i\delta} \right\}, \quad (22)$$

$$B(\mathbf{Q},\mathbf{q},\omega) = -\frac{V_{\mathbf{k}}}{N}\sum_{\mathbf{p}} \frac{1}{\varepsilon_{\mathbf{p}+\mathbf{Q}^*} - \varepsilon_{\mathbf{p}}} \times \frac{f(\varepsilon_{\mathbf{p}+\mathbf{Q}^*})}{(\omega - (\varepsilon_{\mathbf{p}+\mathbf{Q}} - \varepsilon_{\mathbf{p}+\mathbf{Q}^*}) + i\delta)(\omega - (\varepsilon_{\mathbf{p}+\mathbf{Q}} - \varepsilon_{\mathbf{p}}) + i\delta)}. \quad (23)$$

A general form for the effective interaction between the electrons and one impurity located at site $\mathbf{r}_0$ is given by

$$V_{\text{eff}} = \frac{1}{N}\sum_{\mathbf{k}} e^{i\mathbf{k}\cdot\mathbf{r}_0} V_{\mathbf{k}} \sum_{\mathbf{p},\sigma} c^\dagger_{\mathbf{p}+\mathbf{k}\sigma} c_{\mathbf{p}\sigma}. \quad (24)$$

Note that in the presence of N_i randomly distributed impurities, corresponding to an impurity concentration of $n_i = N_i/N$, the neutron scattering spectral weight would be given, in this dilute limit, by

$$\operatorname{Im}\chi_{\text{pure}}(\mathbf{Q},\omega) + N_i\left[\operatorname{Im}\chi(\mathbf{Q},\omega) - \operatorname{Im}\chi_{\text{pure}}(\mathbf{Q},\omega)\right], \quad (25)$$

where $\chi_{\text{pure}}(\mathbf{Q},\omega)$ is the magnetic susceptibility of the pure system and $\chi(\mathbf{Q},\omega)$ is calculated for one impurity using V_{eff} given by Eq. (24).

Below, it will be seen that for $\mathbf{Q}^*$ near $2\mathbf{k}_F$, $\chi_0(\mathbf{Q},\mathbf{q},\omega)$ has a nearly singular structure at $\omega \approx \omega_0$, while for $\mathbf{Q}^*$ away from $2\mathbf{k}_F$, $\chi_0(\mathbf{Q},\mathbf{q},\omega)$ is a smooth function of ω with a small amplitude. Hence, here, the effects of the impurity on $\chi(\mathbf{Q},\omega)$ will be studied by using only the $\pm\mathbf{Q}^*$ components of the effective impurity interaction,

$$V_0 \sum_{\mathbf{p}\sigma} (c^\dagger_{\mathbf{p}+\mathbf{Q}^*\sigma} c_{\mathbf{p}\sigma} + c^\dagger_{\mathbf{p}-\mathbf{Q}^*\sigma} c_{\mathbf{p}\sigma}), \quad (26)$$

where $V_0 = V_{\mathbf{Q}^*}$ is taken as a parameter. This is necessary, since, in order to have sufficient frequency resolution, the calculation needs to be carried out on a large lattice, which is difficult to do using directly Eq. (24). Furthermore, the detailed $\mathbf{k}$ dependence of $V_{\mathbf{k}}$ is not known, especially for $\mathbf{k}$ near $2\mathbf{k}_F$. Here, for simplicity, $\mathbf{k}_F$ will be taken along (1,1). The scattering of a quasiparticle with $\mathbf{Q}^* = 2\mathbf{k}_F$ momentum transfer is sketched in the Brillouin zone in Fig. 5(b). Using the interaction given in Eq. (24), one obtains for $\chi(\mathbf{Q},\omega)$,

$$\chi(\mathbf{Q},\omega) = \left\{\chi_0^{\text{L}}(\mathbf{Q},\omega)(1 - U\chi_0^{\text{L}}(\mathbf{q},\omega)) + 4U(\chi_0(\mathbf{Q},\mathbf{q},\omega))^2\right\} \times \left\{(1 - U\chi_0^{\text{L}}(\mathbf{Q},\omega))(1 - U\chi_0^{\text{L}}(\mathbf{q},\omega)) - 4(U\chi_0(\mathbf{Q},\mathbf{q},\omega))^2\right\}^{-1}, \quad (27)$$

where $\mathbf{q} = \mathbf{Q} - \mathbf{Q}^*$. Here, the factor of 4 multiplying $(\chi_0(\mathbf{Q},\mathbf{q},\omega))^2$ is to take into account the scatterings with momentum transfers $(\pm Q^*, \mp Q^*)$ in addition to $(\pm Q^*, \pm Q^*)$, where $\mathbf{Q}^* = (Q^*, Q^*)$.

In the following, results will be shown for $\langle n\rangle = 0.86$ and $T = 0.05$, in which case $\omega_0 = 2|\mu| \approx 0.55$. Fig. 6(a) shows the real and the imaginary parts of $\chi_0(\mathbf{Q},\mathbf{q},\omega)$ for $\mathbf{Q}^* = 2\mathbf{k}_F$. Here, the Fermi wave vector $\mathbf{k}_F$ has been taken along (1,1) for simplicity. In evaluating $\chi(\mathbf{Q},\omega)$ with Eq. (27), the Lindhard susceptibilities $\chi_0^L(\mathbf{Q},\omega)$ and $\chi_0^L(\mathbf{q}=\mathbf{Q}-\mathbf{Q}^*,\omega)$ are also used and, hence, they are plotted in Figs. 6(b) and (c). Here, one notes the similarity between the ω dependence of $\chi_0(\mathbf{Q},\mathbf{q},\omega)$ and $\chi_0^L(\mathbf{q}=\mathbf{Q}-\mathbf{Q}^*,\omega)$. Both have vanishing spectral weight for $\omega > \omega_0$ because of kinematic constraints.

In Fig. 7, $\mathrm{Im}\,\chi(\mathbf{Q},\omega)$ versus ω obtained from Eq. (27) by using the results of Fig. 6 are shown for different values of U. The solid lines are for $V_0 = 0.05$ and the dashed lines are for $V_0 = 0$ corresponding to the pure case. Here, it is seen that a peak is induced at $\omega_0 \approx 0.55$ by turning on V_0. One also observes that as U is increased, a hump develops below the peak. This is because of the RPA enhancement of χ in the pure case. In a real system, it is expected that this hump will be smaller because of the band-structure effects and the damping of the quasiparticles by the spin fluctuations. In Fig. 8, it is also seen that the impurity contribution to the low frequency part of $\mathrm{Im}\,\chi(\mathbf{Q},\omega)$ increases as U is increased. In addition, in Fig. 6(c) it was seen that $\chi_0(\mathbf{q}=\mathbf{Q}-2\mathbf{k}_F,\omega)$ has sharp structure near ω_0, but this is not responsible for producing the peak in $\mathrm{Im}\,\chi(\mathbf{Q},\omega)$. For instance, taking out the factor of $(1-U\chi_0^L(\mathbf{q},\omega))$ from both the numerator and the denominator in Eq. (27) does not change the structure of $\mathrm{Im}\,\chi(\mathbf{Q},\omega)$.

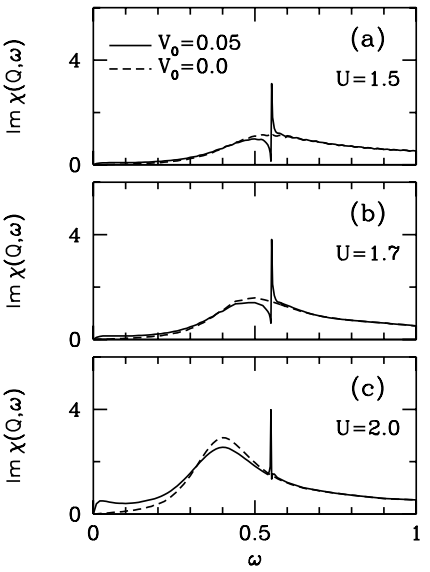

Fig. 7. $\mathrm{Im}\,\chi(\mathbf{Q},\omega)$ versus ω for (a) $U = 1.5$, (b) $U = 1.7$, and (c) $U = 2.0$. These results were for $V_0 = 0.05$ and 0. If the value of V_0 is increased to 0.06, the sharp peak at $\omega_0 \approx 0.55$ diverges.

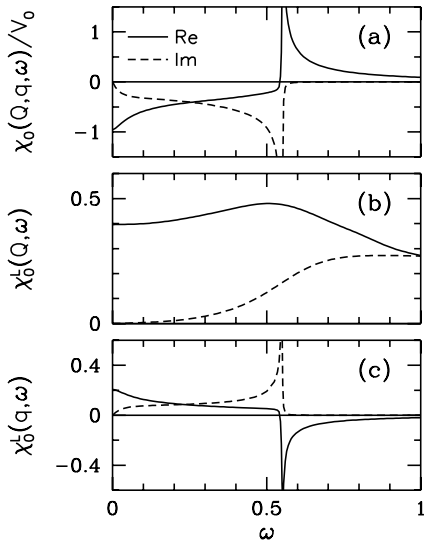

Fig. 6. Frequency dependence of (a) $\chi_0(\mathbf{Q},\mathbf{q},\omega)$ (b) $\chi_0^L(\mathbf{Q},\omega)$ and (c) $\chi_0^L(\mathbf{q},\omega)$. Here $\mathbf{q} = \mathbf{Q} - \mathbf{Q}^*$ and $\mathbf{Q}^* = 2\mathbf{k}_F$. These results were obtained for $\langle n\rangle = 0.86$ and $T = 0.05$.

Next, in order to have a better understanding of these results, a sketch of the important wave vectors and frequencies are given in the $\mathbf{q}$–ω plane in Fig. 8. Here, $\mathbf{Q} = (\pi,\pi)$, and $\mathbf{q}$ and $2\mathbf{k}_F$ are taken along (1,1). The vertical dashed line denotes $\mathbf{q} = \mathbf{Q} - 2\mathbf{k}_F$ and the horizontal dashed line is for $\omega_0 = 2|\mu|$. The shaded area represents the region where $\mathrm{Im}\,\chi_0^L(\mathbf{q},\omega) \neq 0$ at $T = 0$. Here, one observes that the $\mathbf{Q}^* = 2\mathbf{k}_F$ scattering of the $\mathbf{Q} = (\pi,\pi)$ spin fluctuations will lead to a mixing with the $\mathbf{q} = \mathbf{Q} - 2\mathbf{k}_F$ component of the spin fluctuations. A general impurity potential such as Eq. (24) would lead to a mixing with all wave vectors.

Note that the singularity in $\chi_0(\mathbf{Q},\mathbf{q}=\mathbf{Q}-\mathbf{Q}^*,\omega)$ occurs at the upper cut-off of the particle-hole

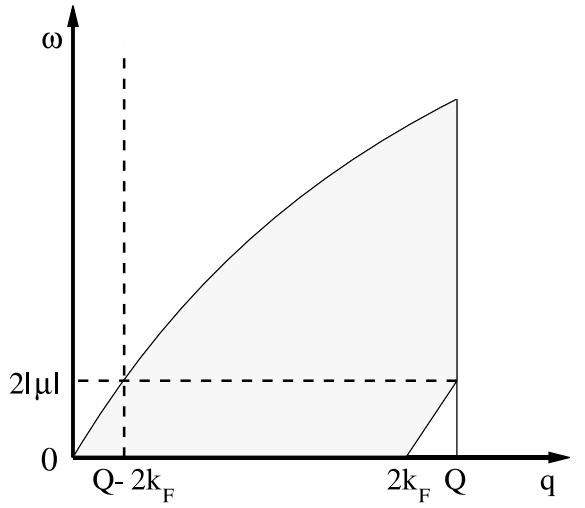

Fig. 8. Sketch (not to scale) in $\mathbf{q}-\omega$ plane of the wave vectors and frequencies which are relevant in this model. The vertical dashed line denotes $\mathbf{q}=\mathbf{Q}-2\mathbf{k}_{\mathrm{F}}$ where $\mathbf{Q}=(\pi,\pi)$ and the horizontal dashed line denotes $\omega_0=2|\mu|$. The shaded area represents the region where $\mathrm{Im}\,\chi_0^{\mathrm{L}}(\mathbf{q},\omega)\neq 0$ at $T=0$. Here $\mathbf{q}$ and $2\mathbf{k}_{\mathrm{F}}$ were taken along $(1,1)$.

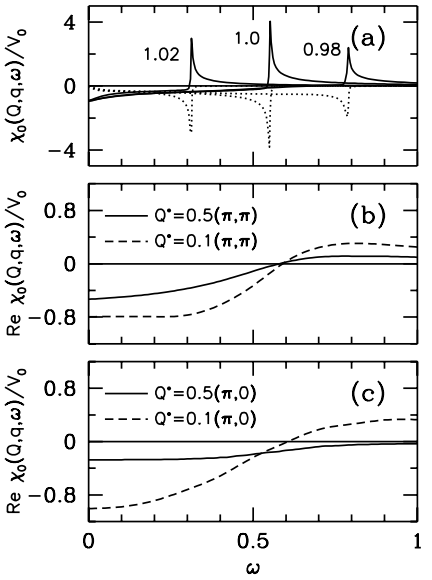

Fig. 9. (a) $\chi_0(\mathbf{Q},\mathbf{q},\omega)/V_0$ versus ω for different values of $\mathbf{Q}^*$ near $2\mathbf{k}_{\mathrm{F}}$ along (1,1). Here, the numbers next to the curves indicate the magnitude of $\mathbf{Q}^*$ in units of $2k_{\mathrm{F}}$. The solid and the dotted curves represent the real and the imaginary parts. In (b) and (c), results on $\mathrm{Re}\,\chi_0(\mathbf{Q},\mathbf{q},\omega)/V_0$ versus ω are plotted for $\mathbf{Q}^*$ away from $2\mathbf{k}_{\mathrm{F}}$.

continuum for the wave vector $\mathbf{q}=\mathbf{Q}-\mathbf{Q}^*$. In this model, the quasiparticle bandwidth determines how much the particle-hole continuum extends in energy, and hence ω_0 occurs at a fraction of the bandwidth W. For the simple tight-binding dispersion that is used here, this cut-off frequency is exactly $2|\mu|$. For more complicated band structures, the singularity in $\chi_0(\mathbf{Q},\mathbf{q}=\mathbf{Q}-\mathbf{Q}^*,\omega)$, if it exists at all, would occur at a frequency which is less than the effective bandwidth W.

In order to show that the nearly singular ω dependence of $\chi_0(\mathbf{Q},\mathbf{q},\omega)$ occurs only for $\mathbf{Q}^*\approx 2\mathbf{k}_{\mathrm{F}}$, in Fig. 9 results on $\chi_0(\mathbf{Q},\mathbf{q},\omega)/V_0$ are shown for various values of $\mathbf{Q}^*$. As seen in Fig. 9(a), for $\mathbf{Q}^*=1.02(2\mathbf{k}_{\mathrm{F}})$, there is a sharp structure in $\chi_0(\mathbf{Q},\mathbf{q},\omega)$ at ω less than ω_0, while for $\mathbf{Q}^*=0.98(2\mathbf{k}_{\mathrm{F}})$, this occurs at $\omega>\omega_0$. As $\mathbf{Q}^*$ moves away from $2\mathbf{k}_{\mathrm{F}}$, the position of the structure in $\chi_0(\mathbf{Q},\mathbf{q},\omega)$ shifts away from ω_0 and its amplitude decreases. In Figs. 9(b) and (c), results on $\mathrm{Re}\,\chi_0(\mathbf{Q},\mathbf{q},\omega)/V_0$ versus ω are shown for $\mathbf{Q}^*$ along (1,1) and (1,0), respectively. Here, $\mathrm{Im}\,\chi_0(\mathbf{Q},\mathbf{q},\omega)/V_0$ is not shown since it is a smooth function of ω with amplitude less than 0.05. In these figures, it is seen that the magnitude of $\chi_0(\mathbf{Q},\mathbf{q},\omega)$ at $\omega\approx\omega_0$ is considerably smaller when $\mathbf{Q}^*$ is away from $2\mathbf{k}_{\mathrm{F}}$. This supports the use of only the $\mathbf{Q}^*$ component of V_{eff} in solving for $\chi(\mathbf{Q},\omega)$. If a general potential such as Eq. (24) instead of Eq. (26) were used in solving for $\chi(\mathbf{Q},\omega)$, then the peak in $\mathrm{Im}\,\chi(\mathbf{Q},\omega)$ would again occur at ω_0 but possibly with a broadened width because of the contributions originating from scatterings with $\mathbf{Q}^*$ away from $2\mathbf{k}_{\mathrm{F}}$.

In Fig. 7, one notes that the line shape of the peak depends on the value of U. For $U=1.5$ and 1.7, the peak is asymmetric; there is a dip below the peak. For $U=2.0$, the dip is not observed. In order to have a better understanding of this, further results on the line shape are shown in Fig. 10(a) and (b) for $U=1.7$ and 2.0, respectively. In these figures, if the value of V_0 is increased to 0.06, the peak at ω_0 diverges. Also shown here in Fig. 10(c) is the quantity

$$\gamma(\omega)=4U^2(\chi_0(\mathbf{Q},\mathbf{q},\omega))^2, \tag{28}$$

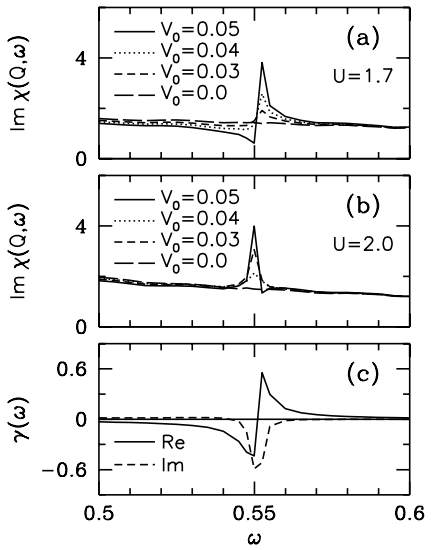

Fig. 10. $\mathrm{Im}\,\chi(\mathbf{Q},\omega)$ versus ω for different values of V_0, and for (a) $U = 1.7$ and (b) $U = 2$. (c) $\gamma(\omega)$ versus ω for $V_0 = 0.05$ and $U = 2.0$. These results were obtained for $\delta = 0.001$.

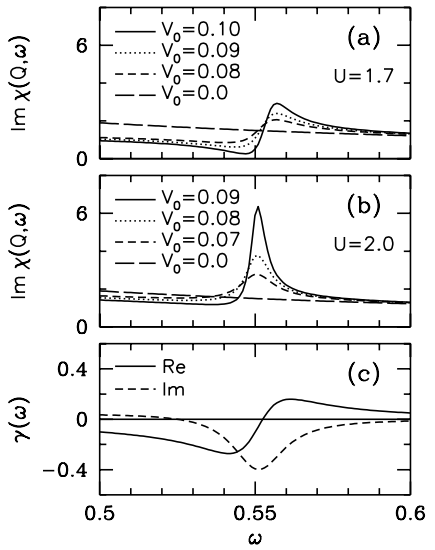

Fig. 11. Results similar to those shown in Fig. 10 but for $\delta = 0.01$. In (c), $V_0 = 0.09t$ was used.

which enters Eq. (27). For $U = 1.7$, the system is away from the magnetic instability and, in this case, $\mathrm{Re}\,\gamma(\omega)$ has a stronger effect than the imaginary part. While for $\omega > \omega_0$, $\mathrm{Re}\,\gamma(\omega)$ leads to a stronger RPA enhancement of $\mathrm{Im}\,\chi(\mathbf{Q},\omega)$, for $\omega < \omega_0$ it suppresses $\mathrm{Im}\,\chi(\mathbf{Q},\omega)$. On the other hand, for $U = 2$, where $1 - U\mathrm{Re}\,\chi_0^{\mathrm{L}}(\mathbf{Q},\omega)$ is small, the pure system is already close to the magnetic instability and $U\mathrm{Im}\,\chi_0^{\mathrm{L}}(\mathbf{Q},\omega)$ acts as a damping of the RPA enhancement. In this case, $\mathrm{Im}\,\gamma(\omega)$ becomes more important and it leads to the peak in $\mathrm{Im}\,\chi(\mathbf{Q},\omega)$ by suppressing the damping of the RPA enhancement. Possibly, this is the case more applicable to $YBa_2Cu_3O_7$.

The results seen in Fig. 10 were obtained using a finite broadening $\delta = 0.001$ in Eqs. (19), (22) and (23). For comparison, results obtained using $\delta = 0.01$ are shown in Fig. 11. In this case, the structure in $\gamma(\omega)$ and the peak in $\mathrm{Im}\,\chi(\mathbf{Q},\omega)$ are broader. It is also seen that the integrated spectral weight in the peak increases with δ for $U = 2$. If δ is increased further, the width of the peak in $\mathrm{Im}\,\chi(\mathbf{Q},\omega)$ and the total spectral weight in it continue to increase for $U = 2$ (not shown here). It is noted that the scattering of the quasiparticles by the spin fluctuations could have an effect similar to that of the finite broadening δ used here. So, in these figures it is observed that the quantitative features of the changes induced by the umklapp processes depend on the model parameters.

4. Discussion

In the normal state, the neutron scattering experiments find that the main effect of the dilute Zn impurities is to induce spectral weight at 40 meV as well as at low frequencies. An important issue is whether the 40 meV peak observed in the experiments corresponds to the peak at ω_0 in $\mathrm{Im}\,\chi(\mathbf{Q},\omega)$ found in this model.

For the simple tight-binding dispersion assumed here one has $\omega_0 = 0.55t$. This value of ω_0 would imply an effective bandwidth W of 0.6 eV. This small value of W would actually be consistent with the results of the Monte Carlo calculations on the single-particle spectrum of the two-dimensional Hubbard model. These calculations [20–22] find that, in the half-filled case, the main features of the single-particle spectrum are the lower and the upper Hubbard bands and two additional

dispersing bands which form at the top of the lower Hubbad band and at the bottom of the upper Hubbard band. The dispersing bands have a bandwidth of about $2J$, where $J \approx 4t^2/U$ is the magnetic exchange, and their dispersion is similar to that of the quasiparticles propagating in a spin-density-wave state. Upon hole doping away from half-filling, spectral weight from above the Mott-Hubbard gap shifts down and the dispersing band which was located at the top of the lower Hubbard band is transformed into a metallic band. For about 13% hole doping, the bandwidth of this metallic band is between $4J$ and $5J$, which would correspond for the layered cuprates to 520 and 650 meV, respectively, if the magnetic exchange J is assumed to be 130 meV.

The ARPES experiments [23] have determined the quasiparticle dispersion in $YBa_2Cu_3O_7$ below the Fermi level and found bonding and antibonding bands which, respectively, extend 0.5 and 0.2 eV below the Fermi level. However, in order to determine the particle-hole continuum and to see whether $\mathrm{Im}\,\chi(\mathbf{Q}, \mathbf{q} = \mathbf{Q} - \mathbf{Q}^*, \omega)$ in this case has any singular behavior, it would be necessary to know the dispersion of the bands above the Fermi level as well.

It is useful to note that in Refs. [24,25] the NMR data on the normal state of $YBa_2Cu_3O_7$ were fitted using a W of 1 eV. It is also useful to compare the value of the spin-fluctuation peak frequency ω_0 found in this paper with the values found for the resonance frequency of the pure system in the d-wave superconducting state. In Ref. [26], where the spin-fluctuation peak of pure $YBa_2Cu_3O_7$ below T_c is attributed to an instability in the magnetic channel, the resonance frequency depends on μ and the magnitude of the d-wave superconducting gap Δ_d as well as U and T, but for the realistic values of Δ_d and of the model parameters, ω_0 takes values close to $2|\mu|$. In Refs. [27,28], the mixing of the magnetic and the particle-particle triplet channels due to the presence of the d-wave superconducting order parameter is also taken into account. In this case, the resonance frequency occurs exactly at $2|\mu|$. However, it is important to keep in mind that these calculations were carried out basically at the level of RPA and there could remain important corrections to the position of the spin-fluctuation peak which are beyond this approximation.

In Section 2 and 3, the results of rather simple model calculations have been given. Clearly, at this point, it is difficult to comment on the origin of why Zn impurities induce a peak in the normal state of $YBa_2Cu_3O_7$. Before any conclusions can be drawn, it is necessary to carry out calculations beyond RPA and the weak-scattering approach. In the calculations, more realistic quasiparticle dispersions need to be employed as well. Furthermore, it would be necessary to study the effects of the Zn impurities below T_c and their relation to the peak induced in the normal state. The purpose of Section 3 has been to explore any consequences of the impurity induced umklapp scatterings on $\mathrm{Im}\,\chi(\mathbf{Q}, \omega)$, which were neglected in Section 2, using a rather general framework.

5. Summary

In summary, the effects of dilute nonmagnetic impurities on the frequency dependence of $\mathrm{Im}\,\chi(\mathbf{Q}, \omega)$ have been studied. These calculations were motivated by the neutron scattering data of Refs. [5,6] on 2% and 0.5% Zn substituted $YBa_2Cu_3O_7$. The origins of the peak and of the low-frequency spectral weight induced by the impurities are the two important questions which are posed by the neutron scattering data.

In pure $YBa_2Cu_3O_7$, a resonant peak is observed only in the superconducting state at $\omega = 41$ meV [8–10]. The width of this peak is resolution limited as opposed to that observed in the Zn substituted samples. The theories attribute the resonant peak of the pure sample to instabilities in the particle–particle [27,28] or the magnetic channels [22]. The calculations presented here for a rather simple model show how a peak in $\mathrm{Im}\,\chi(\mathbf{Q}, \omega)$ could possibly arise from the magnetic channel due to the impurity induced umklapp scatterings in the normal state. However, clearly, higher order calculations are necessary, and the contributions to the peak from other channels are not ruled out.

The calculations presented in this paper have been carried out first without taking into account

the umklapp scattering of the spin fluctuations. Here, the influence of the range of the impurity potential on $\chi_0(\mathbf{Q},\omega)$ has been studied. When a strongly attractive onsite impurity potential is used, it has been found that 2% impurities have a negligible effect on $\chi_0(\mathbf{Q},\omega)$. This is in agreement with the calculations of Ref. [13] in the unitary limit for an onsite potential. When an extended impurity potential is used with parameters similar to those obtained from the exact diagonalization calculations [17], 2% impurities lead to the smearing of $\chi_0(\mathbf{Q},\omega)$ inducing spectral weight at low frequencies. However, for 0.5% impurities a negligible effect is found.

In the third section, the effects of the processes where the spin fluctuations scatter from the impurities with finite momentum transfers were taken into account. It has been shown that the scattering of the spin fluctuations with momentum transfer $\mathbf{Q}^* \approx 2\mathbf{k}_F$ could lead to a peak in $\mathrm{Im}\,\chi(\mathbf{Q},\omega)$ at $\omega \approx \omega_0 = 2|\mu|$. Here, the dependence of the impurity induced changes on the model parameters have been studied. For instance, it was seen that the line shape of the peak depends on the model parameters. When the parameters are such that the Stoner enhancement is small, a dip is observed below the peak. On the other hand, when $1-U\mathrm{Re}\,\chi_0(\mathbf{Q},\omega)$ is small, the dip is not observed and the $2\mathbf{k}_F$ scatterings could lead to a peak in $\mathrm{Im}\,\chi(\mathbf{Q},\omega)$ by suppressing the damping of the RPA enhancement. In addition, in this case, the width of the peak increases with the broadening of the single-particle excitations. It has been also found that the impurity scatterings with finite momentum transfers could lead to spectral weight at low ω.

Finally, in Section 4, a comparison of the results with the experimental data has been given, and the relevant energy scales have been discussed. Here, the need to carry out calculations beyond RPA and the weak-scattering approach has been pointed out. If the results presented here are supported by higher order calculations, then it would mean that a contribution to the peak observed in $\mathrm{Im}\,\chi(\mathbf{Q},\omega)$ could arise from the magnetic channel. Furthermore, it would mean that a perturbation in the density channel as Eq. (26) could induce important changes in the antiferromagnetic response of the system.

Acknowledgements

The author thanks P. Bourges, H.F. Fong and B. Keimer for helpful discussions. The numerical computations reported in this paper were performed at the Center for Information Technology at Koç University.

References

[1] G. Xiao, M.Z. Cieplak, J.Q. Xiao, C.L. Chien, Phys. Rev. B 42 (1990) 8752.
[2] T.R. Chien, Z.Z. Wang, N.P. Ong, Phys. Rev. Lett. 67 (1991) 2088.
[3] A.V. Mahajan, H. Alloul, G. Collin, J.F. Marucco, Phys. Rev. Lett. 72 (1994) 3100.
[4] P. Mendels, J. Bobroff, G. Collin, H. Alloul, M. Gabay, J.F. Marucco, N. Blanchard, B. Grenier, Europhys. Lett. 46 (1999) 678.
[5] Y. Sidis, P. Bourges, B. Hennion, L.P. Regnault, R. Villeneuve, G. Collin, J.F. Marucco, Phys. Rev. B 53 (1996) 6811.
[6] H.F. Fong, P. Bourges, Y. Sidis, L.P. Regnault, J. Bossy, A. Ivanov, D.L. Milius, I.A. Aksay, B. Keimer, Phys. Rev. Lett. 82 (1999) 1939.
[7] L.P. Regnault, in: A. Furrer (Ed.), Neutron Scattering in Layered Copper-Oxide Superconductors, Kluwer, Dordrecht, 1998.
[8] J. Rossat-Mignod, et al., Physica C 185–189 (1991) 86.
[9] H.A. Mook, M. Yethiraj, G. Aeppli, T.E. Mason, T. Armstrong, Phys. Rev. Lett. 70 (1993) 3490.
[10] H.F. Fong, B. Keimer, P.W. Anderson, D. Reznik, F. Dogan, I.A. Aksay, Phys. Rev. Lett. 75 (1995) 316.
[11] P. Hirschfeld, P. Wölfle, D. Einzel, Phys. Rev. B 37 (1998) 83.
[12] S.M. Quinlan, D.J. Scalapino, Phys. Rev. B 51 (1995) 497.
[13] J.-X. Li, W.-G. Yin, C.-D. Gong, Phys. Rev. B 58 (1998) 2895.
[14] J.S. Langer, Phys. Rev. 120 (1960) 714.
[15] G. Mahan, Many Particle Physics, Plenum, New York, 1981.
[16] D. Poilblanc, D.J. Scalapino, W. Hanke, Phys. Rev. Lett. 72 (1994) 884.
[17] D. Poilblanc, D.J. Scalapino, W. Hanke, Phys. Rev. B 50 (1994) 13020.
[18] W. Ziegler, D. Poilblanc, R. Preuss, W. Hanke, D.J. Scalapino, Phys. Rev. B 53 (1996) 8704.
[19] T. Xiang, J.M. Wheatley, Phys. Rev. B 51 (1995) 11721.
[20] N. Bulut, D.J. Scalapino, S.R. White, Phys. Rev. B 50 (1994) 7215.
[21] E. Dagotto, A. Nazarenko, M. Boninsegni, Phys. Rev. Lett. 73 (1994) 728.
[22] R. Preuss, et al., Phys. Rev. Lett. 73 (1994) 732.
[23] M.C. Schabel, et al., Phys. Rev. B 57 (1998) 6091.

[24] N. Bulut, D. Hone, D.J. Scalapino, N.E. Bickers, Phys. Rev. Lett. 64 (1990) 2723.
[25] N. Bulut, D.J. Scalapino, Phys. Rev. Lett. 67 (1991) 2898.
[26] N. Bulut, D.J. Scalapino, Phys. Rev. B 53 (1996) 5149.
[27] E. Demler, S.-C. Zhang, Phys. Rev. Lett. 75 (1995) 4126.
[28] E. Demler, H. Kohno, S.-C. Zhang, Phys. Rev. B 58 (1998) 5719.